| Mitt. naturwiss. Ver. Steiermark | Band 132 | S. 63–82 | Graz 2002 |
|---|---|---|---|

# Relative chronology and absolute age dating of structures related to eo-Alpine high-pressure metamorphism and Oligocene magmatism in the SE Ötztal complex (Texel Group, South Tyrol, Italy)

Von Ulrike Exner*,[1], Bernhard Grasemann[2], Martin Thöni[2] & Christine Miller[3]
Mit 8 Abbildungen und 2 Tabellen

Angenommen am 23. Oktober 2002

**Zusammenfassung: Strukturen im Zusammenhang mit der Eo-Alpinen Metamorphose und dem Oligozänen Magmatismus im südöstlichen Ötztal Komplex (Texel Gruppe, Südtirol, Italien): Relative Zeitabfolge und absolute Altersdatierungen.** – In der vorliegenden Arbeit werden neue strukturelle und geochronologische Daten aus dem Saltausertal in Sütirol (Italien) präsentiert. Die in diesem Gebiet aufgeschlossenen metamorphen Gesteine gehören den polymetamorphen Einheiten des ostalpinen Basements des Ötzal-Komplexes an. Gemeinsam mit dem nördlich anschliessenden Schneebergerzug erfuhr der südöstliche Teil des Ötzal-Komplexes in der Kreide intensive Deformation und druckbetonte Metamorphose. In dieser Zone westlich des Passeiertales sind Metabasite aufgeschlossen, die reliktische eklogitfazielle Mineralparagenesen führen. Die metasedimentären und metagranitoiden Umgebungsgesteine der Eklogit-Amphibolite dokumentieren hauptsächlich amphibolitfazielle Bedingungen, jedoch sind einige wenige Hochdruckphasen in Kernen von Hellglimmer oder Granat erhalten, was auf eine gemeinsame metamorphe Entwicklung dieser Gesteine mit den Metabasiten hinweist. Die Eklogit-Amphibolite bilden unterschiedlich große Boudins innerhalb der umgebenden Ortho- und Paragneise. Die Strukturen in den eoalpin eklogitfaziell geprägten Metabasiten und ihren sauren Umgebungsgesteinen werden mit der Exhumation und Platznahme der Hochdruckgesteine in Verbindung gebracht. Dieser Prozess stellt eine mehrphasige, aber kontinuierliche Entwicklung bei abnehmendem Metamorphosegrad mit unterschiedlichen kinematischen Rahmenbedingungen dar. Die erste penetrative Deformation bildet eine mylonitische Foliation mit einer E-W streichenden Mineralliniation aus. Rb-Sr Datierungen an Hellgimmern aus mylonitischen Orthogneisen, die während dieser Deformation dynamisch rekristallisierten, ergaben Alter um 90 Ma. Diese mylonitische Foliation wird von grossmasstäblichen, südvergenten Falten überprägt, wobei Plagioklas-Wachstum in den Faltenscheiteln auf Temperaturen über 500°C bei dieser Deformation schliessen lässt. Zwei darauffolgende duktile bis sprödduktile Deformationsphasen liefen unter grünschieferfaziellen Bedingungen ab; sie bezeugen geringere finite Deformation in höheren Krustenniveaus. Spröder Versatz an N-S streichenden Störungen steht in Beziehung zu tertiären Bewegungen an der Passeier- und Jaufenlinie. Diese Störungen sind meist mit Pseudotachyliten und Ultrakataklasiten assoziiert, aber manchmal auch mit kühlen Quarz-Ultramyloniten. Diese Deformationsphase wird von der Intrusion eines ca. 3 m mächtigen andesitischen Ganges begleitet. Biotit und Granat aus diesem magmatischen Gestein wurden mit der Rb-Sr- bzw. Sm-Nd-Methode datiert. Die gemessenen Mineralalter liegen um 33–32 Ma und korrelieren gut mit den Altern anderer periadriatischer Intrusiva.

Zusammen mit den eklogitfaziellen Gesteinen in Schober- und Kreuzeckgruppe südlich des Tauernfensters und in Sau- und Koralpe weiter im Osten, bilden Schneebergerzug und die Metabasit-führenden Einheiten des südöstlichen Ötztalkristallins den sogenannten "eoalpinen Hochdruckgürtel". Alle diese Vorkommen liegen in einer ähnlichen tektonischen Position im südlichen ostalpinen Basement, im Norden bzw. Westen der Periadriatischen Linie. Die hier präsentierten strukturgeologischen Daten untermauern eine S-SE gerichtete Extrusion der Hochdruck- bzw. druckbetonten Einheiten des südöstlichen Ötztalkristallins und des Schneebergerzuges während andauernder Konvergenz in einer eoalpinen intrakontinentalen Subduktionszone.

* Corresponding author: ulrike.exner@erdw.ethz.ch
[1] Geologisches Institut, ETH Zürich; Sonneggstr. 5, CH-8092 Zürich (Switzerland)
[2] Institut für Geologie, Universität Wien; Althanstr. 14, A-1090 Wien (Austria)
[3] Institut für Mineralogie und Petrographie, Universität Innsbruck; Innrain 52, A-6020 Innsbruck (Austria)

**Summary:** The present study provides new structural and geochronological data from the Saltaus valley, Southern Tyrol (Italy). The metamorphic rocks exposed in this area are attributed to the polymetamorphic Austroalpine basement units of the Ötztal complex. Together with the northerly adjacent Schneeberg complex, the southeastern part of the Ötztal complex was subjected to intense deformation during the P-dominated Cretaceous metamorphism. Metabasites containing relics of eclogite-facies mineral assemblages are exposed in a zone to the W of the Passeier valley. Metasedimentary and metagranioid host rocks of these eclogite-amphibolites record predominately amphibolite-facies conditions, nevertheless few HP-phases were preserved in the cores of white micas or garnets, suggesting a common metamorphic history with the metabasic rocks. The eclogite-amphibolites form boudins of various dimensions within the ortho- and paragneisses. It is suggested that the structures observed in the eo-Alpine eclogite facies metabasites and their acidic host rocks are related to exhumation and emplacement of the HP-rocks. This process can be described as polyphase but continuous, recording decreasing metamorphic conditions within a varying kinematic frame. The first penetrative deformation forms a mylonitic foliation with an E-W trending mineral lineation. Rb-Sr dating of white mica from mylonitic orthogneisses, which show dynamic recrystallisation during this deformation, gave ages around 90 Ma. This mylonitic foliation is deformed by large-scale, S-vergent folds with plagioclase recrystallizing in fold hinges, indicating T-conditions above 500°C for this deformation. Two subsequent brittle-ductile deformation phases acted under greenschist facies conditions, recording minor finite deformation at shallower crustal levels. Brittle faulting related to Tertiary movements along the Passeier and Jaufen Lines is documented by N-S trending faults, often associated with pseudotachylites and ultracataclasites, but also low-T quartz-ultramylonites. This deformation is accompanied by the intrusion of an andesitic dyke. Biotite and garnet from this 3 m thick magmatic body have been dated by the Rb-Sr and Sm-Nd methods, respectively. The measured mineral ages at 33–32 Ma are well in line with those of other Periadriatic intrusions along the whole Alpine chain.

Together with eclogite-facies rocks in the Schober- and Kreuzeck Gruppe and the Sau- and Koralpe, the Schneeberg complex and the metabasite-bearing units of the SE Ötztal complex are regarded as part of the "eo-Alpine high pressure belt" in the southern Austroalpine basement units. All these occurrences have similar tectonic positions within the southern part of the Austroalpine basement, to the N/W of the Periadriatic lineament. The new structural observations are in favor of a S-SE-directed extrusion of the HP- and P-dominated units of the Schneeberg complex and the SE Ötztal complex during ongoing convergence in an intracontinental Cretaceous subduction zone.

## 1. Regional geologic outline

The Ötztal crystalline complex (ÖC) consists of medium to high-grade metamorphic rocks of varying origin and mineralogical composition. Metasediments, mainly paragneisses are frequently intercalated with metaigneous rocks like orthogneisses and metabasites. The ÖC and the adjacent Silvretta basement (Fig 1.) are part of the Austroalpine tectonic unit and record a polyphase tectonometamorphic history. The major part of these crystalline units preserved a dominantly Variscan metamorphism, but in some places early Palaeozoic rocks have also been preserved (see Thöni 1999 and references cited therein). The Alpine evolution of the SE part of the ÖC unit is subject of this study. It correlates with the main Alpine deformation phases described from the S and W margin of the ÖC (Schmid and Haas 1989; Froitzheim et al. 1997).

The eo-Alpine metamorphic overprint increases from subgreenschist facies in the NW to upper amphibolite facies conditions in the SE (Thöni 1981). Through detailed geochronological work using the Rb-Sr isotopic system of mica in ortho- and paragneisses Variscan ages were obtained in the W and NW part of the ÖC, as well as Variscan-Alpine mixing ages in the lower central part, and a zone of eo-Alpine mica ages (AMA, Fig. 1) in the SE. The Alpine PT-conditions increase towards SE, reaching peak temperatures in the Texel group with eo-Alpine growth of staurolite and kyanite (Purtscheller et al. 1987).

Hoinkes and Thöni (1987) first described eclogitic parageneses within the zone of eo-Alpine amphibolite facies metamorphism. A more detailed study of these eclogites revealed a complex history with Cretaceous minimum peak pressures of 1.1–1.2 GPa at 500–550°C, followed by temperature increase and contemporary pressure release, and

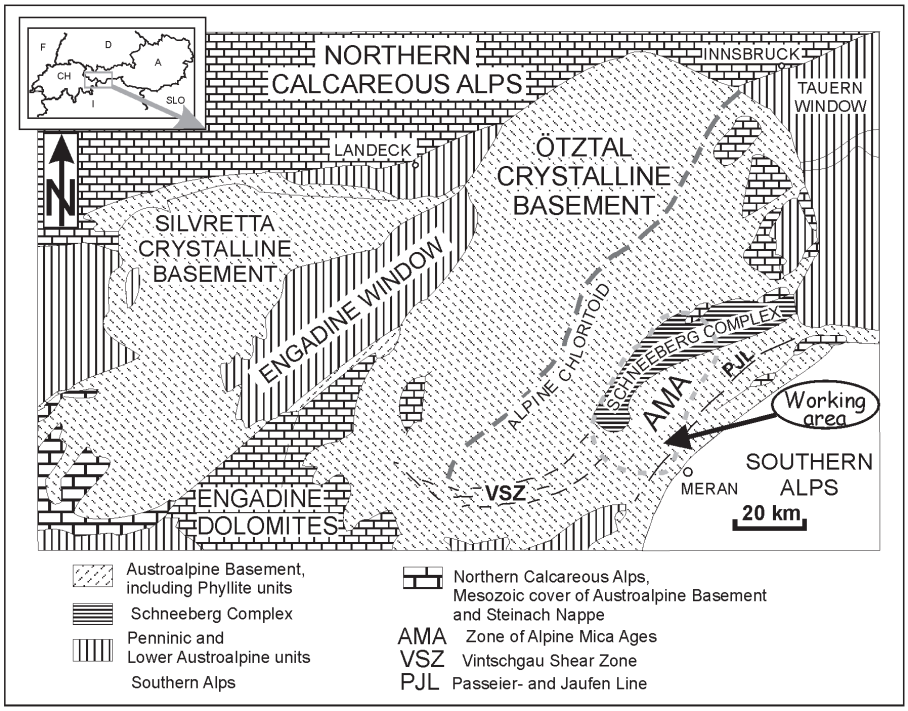


Fig. 1: Tectonic sketch map of Ötztal basement and surrounding areas. The study area lies in the southeastern part of the Ötztal Crystalline basement, within the zone of Alpine mica ages (AMA).

subsequent exhumation and cooling (Hoinkes et al. 1991). However, during an intense amphibolite-facies overprint after peak pressure conditions the Rb-Sr isotopic system in micas has been completely reset. Conclusive geochronological data from the high-P assemblages have not been obtained so far, and the precise age of eo-Alpine HP-metamorphism has not yet been defined (Hoinkes et al. 1991, Sölva et al. 2001). Additional petrological and structural data on the HP-metamorphism were collected in the vicinity of the eclogites by Spalla (1990, 1993), who concluded that all structures in the metapelitic rocks of the Spronser valley are of Alpine age and related to the exhumation of the subducted basement. Sölva et al. (2001) presented a detailed geochronological, petrological and structural work on the area north of the Fals valley and described mostly metapelitic and some metabasic rocks that lack any records of HP-metamorphism (>10 GPa), recording mainly upper amphibolite facies mineral assemblages. The eo-Alpine eclogites in the SE ÖC are restricted to a narrow zone close to the Passeier valley, which is bordered by an area of lower eo-Alpine metamorphic conditions in the NW and a zone of Alpine lowest greenschist-facies conditions in the E and SE (Spiess 1995).

After eo-Alpine high-pressure metamorphism, the Austroalpine basement complex was affected by magmatic activity indicated by the intrusion of plutons and dykes along the Periadriatic Line. Traditionally, the Periadriatic Line is interpreted as a first order tectonic boundary between the Southern Alps, which show only minor S-vergent folding and top-to-S thrusting, and the Western and Eastern Alps, dominated by intense top-to-W and N movements. The Periadriatic plutons lack any evidence for eo-Alpine metamorphism and have therefore been regarded as "post-collisional" plutons, formed as a consequence of thermal relaxation after subduction during an intermediate phase of

extension (e.g. Dal Piaz et al. 1988). Geochronological investigations on Periadriatic plutons and dykes revealed intrusion-ages around 30 Ma, indicating a pronounced magmatic activity during a rather short period in the Oligocene. Some occurrences of this magmatic zone, however, have yielded Permian ages (see Thöni 1999 for a review). Most of the Tertiary magmatic bodies intruded into the Austroalpine units, i.e. N of the Periadriatic Lineament. Several models for emplacement of these magmatic bodies were developed, e.g. subduction zone melting, lithospheric extension or thermal boundary layer detachment (see von Blanckenburg et al. 1998 for details). Recent studies are in favor of "compressional magmatism" as regional regime for the formation of the Periadriatic melts (e.g. Hollister and Crawford 1986, Rosenberg et al. 1995). Geochemical analyses of several Periadriatic plutons indicate that both lithospheric mantle melts and crustal sources were involved in the genesis of these magmas. Therefore, the emplacement of melts in convergent orogens prior to the onset of large-scale extension is no longer thought to be in contradiction to tectonic models, as strike-slip and transpressive faulting seems to facilitate segregation and movement of melts (Steenken et al. 2000).

Recent studies provide detailed data on dykes and fault-related rocks from the PAF (Müller et al. 2001), indicating that Oligocene magmatism acted contemporaneously with strike-slip faulting. Age determinations point to long-lasting tectonic activity along the PAF with a complex history pre- and postdating the emplacement of the plutons and dykes, from the Cretaceous up to early Miocene.

## 2. Petrography

Mineral composition data were obtained with an ARL SEMQ microprobe by energy- and/or wavelength-dispersive spectrometry at the University of Innsbruck. The accelerating voltage was 15 kV and sample current 20 nA. Natural and synthetic standards were used for calibration (details are given in Miller et al. 1999). Abbreviations for minerals are after Kretz (1983), additionally: Fsp for feldspar, Wm for white mica.

### 2.1 Orthogneisses

In the area of the Saltauser and Falser valleys (Fig. 2) three types of orthogneisses can be distinguished:

Wm-orthogneisses form concordant layers, ranging from a few cm to some m in thickness, within paragneisses and micaschists. Wm, Fsp, Qtz and sometimes Grt can be identified macroscopically forming the main mineral phases. A weak foliation ($S_{n+2}$) is defined by Wm-dominated and Qtz-Fsp dominated layers, as well as by planar orientation of Wm. In places where this foliation is well developed, a crenulation cleavage overprinting the first foliation was formed during $D_{n+3}$. In thin section, Wm-orthogneiss shows an equigranular, coarse-grained fabric with a weak foliation. Wm-orthogneisses have varying amounts of Kfs. The anhedral Kfs-grains frequently show Mc-hatched twins and perthitic exsolution lamellae. Plagioclase forms xenomorphic grains, which often show (sometimes bent) twins. In some samples Pl represents the dominant Fsp-phase. Usually, two different grain sizes of Wm can be identified: large grains up to 1cm in diameter are aligned parallel to $S_{n+2}$, whereas a large number of much smaller grains is oriented parallel to a new foliation ($S_{n+3}$). A phengitic composition (Hoinkes et al. 1991) can be assumed for at least the cores of large Wm-grains. Garnet occurs in Wm-orthogneisses forming up to 5 mm-sized grains. They have a skeletal grain-shape, i.e. they are extremely inclusion-rich and xenomorphic, suggesting Grt-growth only at grain boundaries of Qtz and Fsp. Large Qtz-grains show undulatory extinction, irregular grain

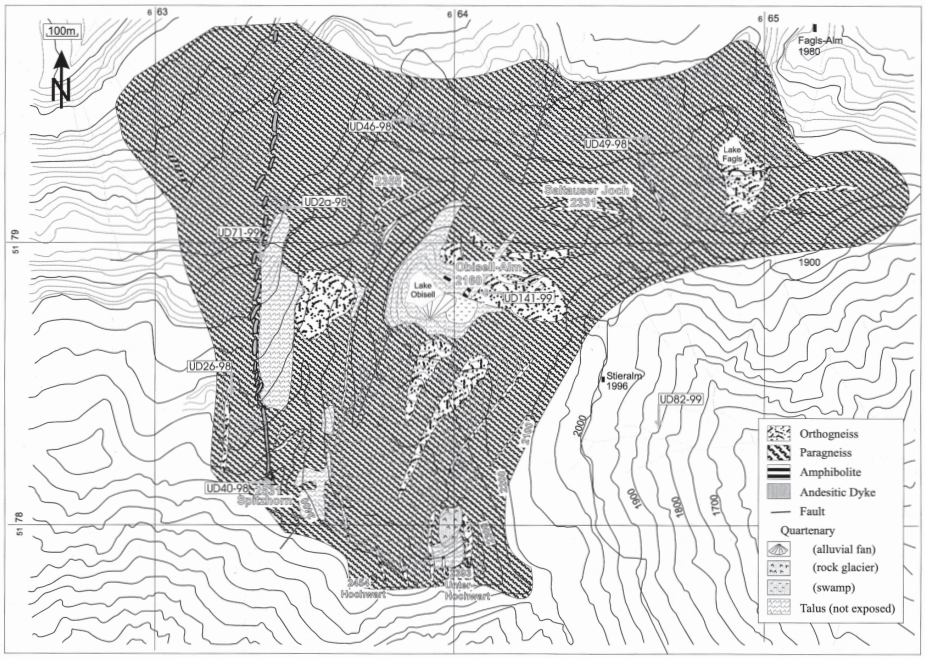


Fig. 2: Geological map of upper Saltaus valley with sample locations.

boundaries and deformation lamellae. Ap, Zrn and Bt can be found as accessory minerals within Wm-orthogneisses.

Bt-Wm-orthogneisses forms large stocks, which are intensely deformed at their rims and less deformed at the center. They have large Kfs with preserved magmatic twins, as well as Bt-aggregates which are also characteristic of the large Tschigot orthogneiss body (Helbig and Schmidt 1978) in the SW vicinity of the study area. Additional mineral phases are Qtz and Wm. Kfs forms up to several cm large grains with magmatic Carlsbad twins. Perthitic exsolution lamellae and myrmekites are common. Large grains recrystallised dynamically at their rims, often forming new Pl-(sub)grains. Large Bt-aggregates are characteristic of Tschigot-type-orthogneisses. Bt forms a foliation ($S_{n+2}$), which is also defined by alternating mica-rich and Qtz-Fsp-rich layers. Bt-grains are up to 3 mm in diameter and sometimes show alteration to Chl. Wm occurs together with Bt in clusters and layers. The grain size is identical to that of Bt but Wm shows only rarely intergrowth with Bt. Qtz often forms layers with large elongate grains. These grains show (sometimes patchy) undulatory extinction, irregular grain boundaries and subgrains. Ap occurs as up to 1 cm large euhedral clasts. Other common accessory minerals are Ep and Zrn.

Bt-Am-orthogneisses occurring close to the eclogite-amphibolites and amphibolites differ from the two types described above because of their considerable Am-content. The up to a few mm long, acicular Am-blasts grow parallel to the foliation ($S_{n+2}$), but show a random orientation with respect to the lineation ($L_{n+2}$). This type of orthogneisses is characterised by a strong planar fabric, which is defined by mm-thick alternating layers of Bt-Am and Qtz-Fsp, respectively. In contrast to the other two orthogneiss-types, this lithology always shows a pronounced mineral lineation, which is defined by Qtz, Fsp and Bt. Pl is the only Fsp-phase in Bt-Am-orthogneisses, forming anhedral grains in Qtz-rich layers. In monomineralic Qtz-ribbons large grains have formed by grain boundary

migration. These large grains were again deformed, developing subgrains, irregular grain boundaries and undulatory extinction. In Pl-Qtz-layers both minerals show equidimensional grains with triple junctions. Anhedral Ep and Czo are common, as well as Ap, sphene and Zrn.

### 2.2 Metapelites

Monotonous paragneisses containing Bt, Qtz and Pl (minor Wm and Grt) and Grt-Pl-bearing, Wm-rich micaschists are the dominant lithologies.

In micaschists several Grt-generations can be distinguished: **Grt1** was only found in one sample (UD46–98). It forms the core of large (2–5 mm) Grt-porphyroblasts, and shows inclusions of fine-grained pigment (presumably Gr) tracing the shape of a former euhedral grain. This may represent an early stage of metamorphism, when the matrix still contained fine-grained pigment (Fig. 3a). **Grt2:** An inner rim of Grt in the same thin section (UD46–98) and the internal zones of many other Grt-grains in similar samples are characterised by coarse-grained inclusions of Wm, Ttn and Qtz. Grt2 is interpreted as being syn- to postkinematic relative to $S_{n+2}$. **Grt3** forms the outer rim of Grt-porphyroblasts. It is partly euhedral, but can be resorbed in strain caps. The main foliation ($S_{n+3}$) curves around Grt3, therefore it is interpreted as pre- to syn- $S_{n+3}$.

St is found in micaschists with variable contents of Qtz, Pl, Wm, Grt ± Bt ±Ky. It forms sometimes euhedral (Fig. 3b) but more often xenomorphic grains, which show a typical light to dark yellow pleochroism. A foliation defined by inclusion trails of Gr, Wm and Zrn is preserved inside the St-porphyroblasts, which is interpreted as $S_{n+2}$. The type and arrangement of inclusions in St and its position within the $S_{n+3}$ foliation is similar to the one in Grt2 and Pl, which are therefore regarded as being formed contemporaneously. Neither the distribution of St-porphyroblasts nor any other features inside the St crystals point to a polyphase growth of this mineral. In fact, St passively rotated into a position parallel to $S_{n+3}$, and did not recrystallise or grow in this position. Most crystals are anhedral, sometimes due to resorption at the rims. Only some grains of the matrix or enclosed in Pl (sample UD26–98) have an euhedral shape. The St-crystals show a varying degree of replacement by very fine-grained Wm and sometimes Chl. These pseudomorphs are not affected by $S_{n+3}$, only in some places a few very small Wm-fibres grow parallel to $S_{n+3}$. Therefore the alteration of St must have taken place late- to post- $D_{n+3}$. St can in some places bear inclusions of Grt. Most probably, Grt2 started to grow somewhat earlier than St and is therefore enclosed within St.

Ky usually forms porphyroblasts up to 2 mm in diameter. Bt is the only mineral phase enclosed in Ky. Pigment trails like those described in Grt or St, were not observed. Nevertheless, due to intergrowth with St and the analogue structural position with respect to $S_{n+3}$, Ky is regarded as syn- to post- $D_{n+2}$. Like St, Ky shows retrograde alteration to fine-grained sericitic Wm, which does not have a preferred orientation. Some domains are characterised by very large (5–7 mm) Ky, and large St crystals, making up nearly the entire rock volume, beside of minor Wm, Bt, Pl and Qtz. In this zone, some Ky blasts show tight folds, undulatory extinction and kinking. Kinking does not occur in Bt-grains, thus indicating that Bt still recrystallised after the deformation of Ky. This observation shows that Ky was deformed by folding under lower amphibolite-facies and kinking under upper greenschist-facies conditions.

Pl forms porphyroblasts, which rotate and recrystallise to a varying degree during $D_{n+3}$. These clasts show inclusions of pigment and Wm, which define an earlier foliation. In some cases, this foliation is curved, and therefore interpreted as an axial plane cleavage of an earlier deformation phase ($D_{n+2}$). During $D_{n+3}$, dynamic recrystallisation of Pl in $S_{n+3}$ takes place, in some cases growth of Pl in $D_{n+3}$–fold hinges can be observed.

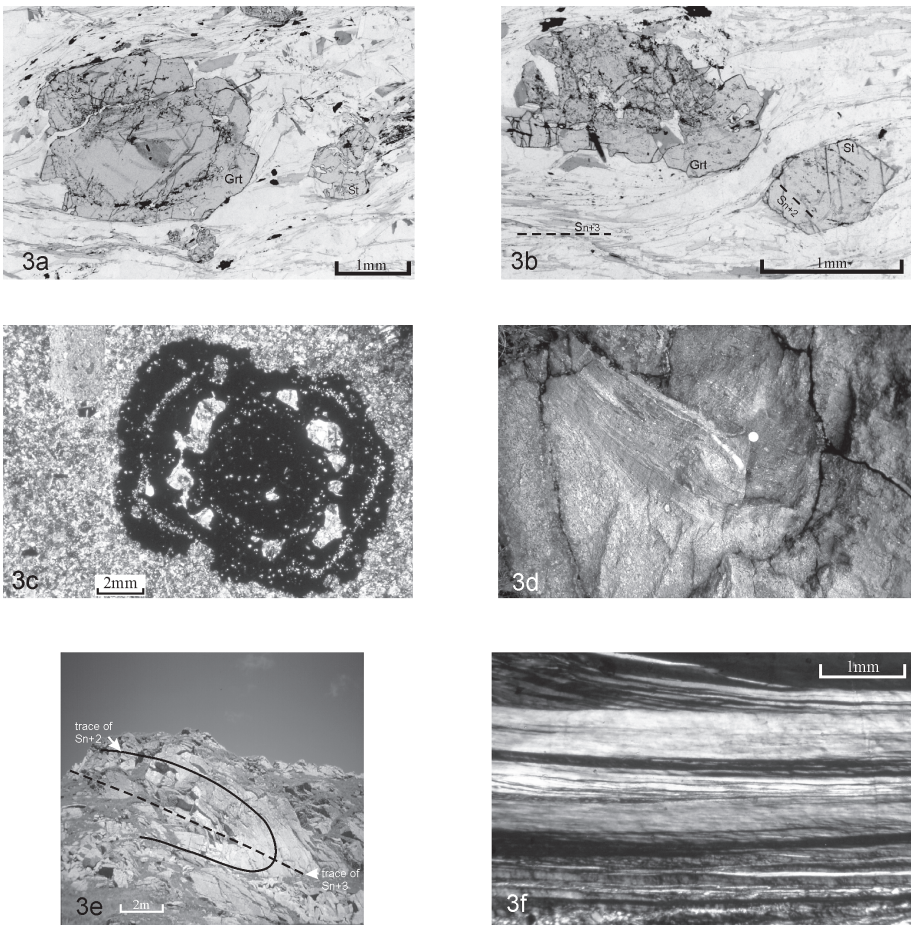


Fig. 3: (a) Thin section of micaschist-sample (UD46–98), showing fine-grained pigment tracing idiomorphic rim of Grt1 in core of large Grt-crystal. (b) Idiomorphic St aligned parallel to $S_{n+3}$, with internal foliation $S_{n+2}$ (sample UD46–98). (c) Well preserved, large Grt-crystal in strongly altered andesitic dyke (Crossed nicols; sample UD2a-98). (d) $D_{n+2}$ shear zone in Bt-Wm orthogneiss. Coin for scale. (e) Large, S-vergent $D_{n+3}$ fold in Wm-orthogneiss (N is to the right). (f) Qtz-ultramylonite with extremely elongated "grains" indicating $D_{n+6}$ deformation (sample UD82–99, crossed nicols).

The paragneisses in the Saltaus and Fals valley have varyable contents of Wm and Bt. In St-Ky-Grt-micaschists, Wm is the dominant mica phase, whereas Bt ± Grt-paragneisses are dominated by Bt. Wm and Bt recrystallise and grow in $S_{n+3}$. Both show inclusions of Gr, similar to those in Pl, St or Grt2.

Qtz forms inclusions in Grt2, where the grains trace an earlier foliation. During $D_{n+3}$ Qtz-grains in the matrix must have recrystallised dynamically, but due to subsequent static grain growth and annealing, the structures were not preserved. Undulatory extinction and irregular grain boundaries indicate a later stage of dynamic recrystallisation at greenschist facies conditions.

Within metapelites, two generations of Chl can be identified. A Mg-rich Chl, showing light-brown colors and typical brown interference colors, is aligned parallel to

$S_{n+3}$, probably in equilibrium with at least the matrix minerals (Wm, Bt, Pl, Qtz),. A later generation of Chl replaces Grt, Bt, Wm and sometimes St and Ky. The decomposition of the latter two mineral phases probably correlates with Ser-formation at the expense of St and Ky. The second Chl-generation is characterised by intense green pleochroism and random orientation.

Ap, Zrn, Ep, Ilm are common accessory phases in micaschists and paragneisses. Tur is another common accessory mineral in micaschists. It forms sometimes up to 3–5 cm large, elongated black crystals, which can be aligned parallel to $S_{n+3}$. Other Tur-crystals are post-tectonic, relative to $D_{n+3}$, with inclusions of medium-grained Grt-crystals, Rt, Ttn, Pl, Wm and Zrn. Rt-crystals enclosed in St-, Ky- and Fsp-porphyroblasts can frequently be observed. Moreover, in the matrix Rt is surrounded by Ilm, which documents a decompression reaction.

### 2.3 Metabasites

Eclogite-amphibolites and amphibolites form cm to dm wide boudinaged layers and boudins, several meters thick, within metapelites and orthogneisses.

Eclogite-amphibolites contain blue-green pleochroic Am-crystals defining a foliation and lineation. Pl-Am symplectites after Px represent the post-eclogitic amphibolite-facies metamorphic stage in these rocks. Grt forms sometimes euhedral grains with inclusion-rich (e.g. Qtz, Rt, Wm, Zrn) cores and inclusion-poor rims. Most Grt-crystals are surrounded by globular symplectite of blue-green Am in Qtz. Zo and phengitic Wm occurs as a member of the HP-paragenesis. Wm is surrounded and often completely replaced by fine-grained symplectites consisting of vermicular Bt and Pl. Zo also forms large (~4 mm) porphyroblasts within Qtz-rich layers. Czo also preserved an internal foliation outlined by the linear orientation of inclusions of (phengitic) Wm. Coarse-grained Pl can be found, which overgrows the HP-assemblage (Am, Omp, Grt, Czo, Ttn) statically. Strain-free Qtz-grains form more or less monomineralic layers within eclogite-amphibolites, documenting that temperatures above 300 °C outlasted deformation in these rocks. Dol, Ttn, Ep, Rt and opaque minerals are typical accessory minerals in eclogite-amphibolites.

Within the amphibolites, Am defines again the main foliation and lineation. Two-stage Grt growth can be observed in amphibolites: The cores of large (3–4 mm) Grt grains show randomly oriented, fine-grained inclusions of Qtz, Ttn, Ap and opaque minerals. The rims bear only few coarse-grained inclusions of the same mineral phases and have an euhedral grain shape. Grt grains form porphyroblasts in the Am-Bt-Qtz-Pl matrix. Grt is replaced by Chl along cracks and veins during a retrograde stage postdating the Grt-formation. Bt is aligned parallel to the main foliation $S_{n+2}$ in amphibolites (built up by Am). It is also common at shear band-planes. Bt grows within strain shadows of Grt-porphyroblasts and is often replaced by Chl. Plagioclase forms anhedral grains within Qtz-rich layers of amphibolites. It is often partially replaced by Ser. Apart from variable contents of anhedral Qtz in the matrix, Qtz forms inclusions in Grt, often tracing an older internal foliation. In addition, Qtz is concentrated in strain shadows around Grt-porphyroblasts. Qtz often shows undulatory extinction, irregular grain boundaries and deformation lamellae. Aphibolites have Ep, Zrn, Ap, Ttn, Rt, and sometimes carbonatic material (probably Dol) as accessory minerals.

### 2.4 Andesitic dyke

An unfoliated, 3 m thick dyke discordantly crosscuts the amphibolite-facies metamorphic rocks of the Saltaus and Fals valleys. Am forms approximately 0.5 cm sized,

Tab. 1: Microprobe analyses of Grt, Fsp, Ilm, Am and Bt from andesitic dyke.

| Sample | UD2a-98 | UD2a-98 | UD2a-98 | UD2a-98 | UD2a-98 | UD40-98 |
|---|---|---|---|---|---|---|
| Analysis | Grt M=62 | Grt rim 1 (0µ) | Grt rim 2 (12000µ) | Grt (9000µ) | Grt core | Grt xeno-morphic |
| SiO2 | 37.93 | 37.71 | 37.50 | 37.90 | 37.93 | 37.93 |
| TiO2 | 0.06 | 0.06 | 0.06 | 0.04 | 0.05 | 0.11 |
| Al2O3 | 21.24 | 21.25 | 21.19 | 21.32 | 21.33 | 21.29 |
| Cr2O3 | 0.02 | 0.05 | 0.06 | 0.02 | 0.00 | 0.03 |
| FeO | 28.64 | 28.15 | 28.56 | 28.91 | 26.80 | 28.35 |
| MnO | 2.69 | 3.97 | 2.71 | 2.88 | 2.24 | 2.49 |
| MgO | 4.23 | 3.46 | 3.59 | 4.29 | 4.00 | 4.31 |
| CaO | 5.37 | 5.36 | 5.60 | 4.70 | 7.44 | 5.75 |
| Total | 100.18 | 100.01 | 99.27 | 100.06 | 99.79 | 100.26 |
| Si | 2.995 | 2.997 | 2.997 | 2.998 | 2.994 | 2.989 |
| Ti | 0.004 | 0.004 | 0.004 | 0.002 | 0.003 | 0.007 |
| Al | 1.977 | 1.991 | 1.996 | 1.988 | 1.985 | 1.978 |
| Cr | 0.001 | 0.003 | 0.004 | 0.001 | 0.000 | 0.002 |
| Fe3+ | 0.023 | 0.005 | 0.000 | 0.010 | 0.018 | 0.024 |
| Fe2+ | 1.869 | 1.866 | 1.909 | 1.903 | 1.752 | 1.844 |
| Mn | 0.180 | 0.267 | 0.183 | 0.193 | 0.150 | 0.166 |
| Mg | 0.498 | 0.410 | 0.428 | 0.506 | 0.471 | 0.506 |
| Ca | 0.454 | 0.456 | 0.480 | 0.398 | 0.629 | 0.486 |
| Total | 8.001 | 8.000 | 8.000 | 8.000 | 8.001 | 8.002 |
| XMg | 0.210 | 0.180 | 0.183 | 0.210 | 0.212 | 0.215 |
| alm | 62.31 | 62.23 | 63.64 | 63.44 | 58.44 | 61.56 |
| py | 16.60 | 13.67 | 14.26 | 16.86 | 15.70 | 16.9 |
| grs | 13.77 | 14.67 | 15.63 | 12.63 | 19.96 | 14.57 |
| sps | 5.93 | 8.89 | 6.12 | 6.42 | 4.86 | 5.33 |
| adr | 1.14 | 0.25 | 0.00 | 0.50 | 0.88 | 1.22 |

**Feldspar**

| Sample | UD40-98 | UD40-98 | UD40-98 | UD40-98 | UD2a-98 |
|---|---|---|---|---|---|
| Analysis | Pl core (1.1) | Pl rim (1.4) | Pl in matrix (3.13) | Pl incl. in Grt | Kfs incl. in Grt |
| SiO2 | 48.14 | 56.76 | 46.55 | 49.94 | 64.22 |
| Al2O3 | 32.57 | 27.41 | 34.16 | 31.49 | 18.42 |
| FeO | 0.33 | 0.23 | 0.36 | 0.40 | 0.30 |
| CaO | 15.74 | 9.49 | 17.46 | 14.53 | 0.26 |
| Na2O | 2.38 | 6.07 | 1.53 | 3.11 | 0.21 |
| K2O | 0.14 | 0.30 | 0.03 | 0.16 | 16.24 |
| Total | 99.30 | 100.26 | 100.09 | 99.63 | 99.65 |
| Cations / 8 Oxygens | | | | | |
| Si | 2.220 | 2.544 | 2.139 | 2.287 | 2.984 |
| Al | 1.770 | 1.448 | 1.850 | 1.700 | 1.009 |
| Fe3+ | 0.011 | 0.008 | 0.012 | 0.014 | 0.010 |
| Ca | 0.778 | 0.456 | 0.860 | 0.713 | 0.013 |
| Na | 0.213 | 0.527 | 0.136 | 0.276 | 0.019 |
| K | 0.008 | 0.017 | 0.002 | 0.009 | 0.963 |
| Total | 5.000 | 5.000 | 4.999 | 4.999 | 4.998 |
| an | 77.87 | 45.56 | 86.16 | 71.41 | 1.30 |
| ab | 21.31 | 52.73 | 13.66 | 27.66 | 1.90 |
| or | 0.82 | 1.72 | 0.18 | 0.94 | 96.80 |

**Ilmenite**

| Sample | UD40-98 | UD40-98 | UD2a-98 | UD70-99 |
|---|---|---|---|---|
| Analysis | Ilm matrix (2.14) | Ilm incl. in Grt (2.2) | Ilm incl. in Grt (65) | Ilm in matrix (1.15) |
| TiO2 | 51.390 | 50.620 | 52.240 | 51.700 |
| Cr2O3 | 0.000 | 0.000 | 0.080 | 0.100 |
| V2O3 | 0.400 | 0.490 | 0.340 | 0.280 |
| FeO | 43.420 | 43.600 | 42.560 | 43.940 |
| MnO | 4.180 | 4.280 | 4.450 | 3.700 |
| NiO | 0.310 | 0.210 | 0.000 | 0.000 |
| Total | 99.700 | 99.200 | 99.670 | 99.720 |
| Ti | 0.982 | 0.973 | 0.995 | 0.987 |
| Cr | 0.000 | 0.000 | 0.002 | 0.002 |
| V | 0.008 | 0.010 | 0.007 | 0.006 |
| Fe3+ | 0.010 | 0.017 | 0.000 | 0.006 |
| Fe2+ | 0.913 | 0.915 | 0.902 | 0.927 |
| Mn | 0.090 | 0.093 | 0.095 | 0.080 |
| Ni | 0.006 | 0.004 | 0.000 | 0.000 |
| Total | 2.009 | 2.012 | 2.001 | 2.008 |

**Amphibole**

| Sample | UD40-98 | UD40-98 | UD40-98 | UD40-98 | UD40-98 | UD70-99 | UD70-99 |
|---|---|---|---|---|---|---|---|
| Analysis | small Amp (3.10-3.12) | Amp 3.1vs. Matrix | Amp 3.3vs. Core | Amp 3.4vs. Rim | Amp 3.6 Core | Amp 1.3 core | Amp 1.2 rim |
| SiO2 | 43.91 | 43.23 | 43.11 | 43.04 | 43.48 | 42.80 | 44.58 |
| TiO2 | 1.74 | 2.12 | 2.06 | 1.81 | 1.84 | 1.41 | 1.53 |
| Al2O3 | 11.25 | 11.58 | 13.26 | 13.45 | 14.13 | 12.42 | 10.16 |
| Cr2O3 | 0.10 | 0.05 | 0.10 | 0.25 | 0.03 | 0.24 | 0.00 |
| FeO | 16.76 | 16.62 | 11.43 | 7.60 | 8.93 | 18.08 | 18.03 |
| MnO | 0.43 | 0.11 | 0.12 | 0.03 | 0.11 | 0.26 | 0.51 |
| MgO | 11.17 | 11.21 | 13.81 | 16.20 | 15.34 | 9.44 | 11.07 |
| CaO | 10.19 | 10.41 | 11.38 | 11.41 | 11.09 | 10.96 | 10.18 |
| K2O | 0.48 | 0.58 | 0.80 | 1.01 | 0.89 | 0.70 | 0.47 |
| Na2O | 1.62 | 1.69 | 1.94 | 2.07 | 1.99 | 1.61 | 1.58 |
| Total | 97.650 | 97.600 | 98.010 | 96.870 | 97.830 | 97.920 | 98.110 |
| Formel | 23 O | 23 O | 23 O | 23 O | 23 O | 23 O | 23 O |
| Cat.Sum-K-Na = 13 | | | | | | | |
| Si | 6.374 | 6.293 | 6.182 | 6.149 | 6.148 | 6.306 | 6.461 |
| Ti | 0.192 | 0.236 | 0.224 | 0.197 | 0.195 | 0.160 | 0.165 |
| Al IV | 1.626 | 1.707 | 1.818 | 1.851 | 1.852 | 1.694 | 1.539 |
| Al VI | 0.301 | 0.280 | 0.423 | 0.416 | 0.500 | 0.467 | 0.194 |
| Cr | 0.009 | 0.009 | 0.009 | 0.026 | 0.000 | 0.027 | 0.000 |
| Fe3+ | 1.218 | 1.108 | 0.742 | 0.770 | 0.896 | 0.844 | 1.310 |
| Fe2+ | 0.814 | 0.914 | 0.629 | 0.140 | 0.157 | 1.388 | 0.876 |
| Mn | 0.052 | 0.018 | 0.017 | 0.000 | 0.017 | 0.035 | 0.061 |
| Mg | 2.415 | 2.434 | 2.958 | 3.452 | 3.235 | 2.073 | 2.395 |
| Ca | 1.587 | 1.628 | 1.750 | 1.743 | 1.681 | 1.727 | 1.585 |
| K | 0.087 | 0.105 | 0.147 | 0.18 | 0.161 | 0.133 | 0.087 |
| Na | 0.453 | 0.481 | 0.543 | 0.575 | 0.543 | 0.461 | 0.444 |
| Cat.Sum | 15.128 | 15.213 | 15.442 | 15.499 | 15.385 | 15.315 | 15.117 |

**Biotite**

| Sample | UD70-99 | UD70-99 |
|---|---|---|
| Analysis | Bt core (1.11) | Bt rim (1.13) |
| SiO2 | 36.13 | 35.85 |
| TiO2 | 4.44 | 3.65 |
| Al2O3 | 14.56 | 15.32 |
| Cr2O3 | 0.00 | 0.00 |
| FeO | 17.54 | 18.08 |
| MnO | 0.11 | 0.12 |
| MgO | 12.07 | 12.19 |
| CaO | 0.09 | 0.11 |
| Na2O | 0.67 | 0.74 |
| K2O | 9.21 | 9.08 |
| Total | 94.82 | 95.14 |
| Cations / 11 Oxygens | | |
| Si | 2.757 | 2.732 |
| Ti | 0.255 | 0.209 |
| Al IV | 1.243 | 1.268 |
| Al VI | 0.068 | 0.108 |
| Cr | 0.000 | 0.000 |
| Fe3+ | 0.000 | 0.000 |
| Fe2+ | 1.120 | 1.152 |
| Mn | 0.007 | 0.008 |
| Mg | 1.409 | 1.412 |
| Ca | 0.008 | 0.009 |
| Na | 0.102 | 0.112 |
| K | 0.920 | 0.901 |
| XMg | 0.551 | 0.546 |

black euhedral crystals, whereas Grt typically occurs as up to 2.5 cm large xenomorphic grains of red color. Bt is rare and forms euhedral dark brown hexagons. Some crosscutting veins were found, filled with white Ep-minerals and Qtz. Alm-rich Grt, tschermakitic Am, An-rich Pl and Ti-rich Bt form phenocrystals in a fine-grained, Pl-rich matrix (compositional data are given in Tab. 1). Phenocrysts and matrix have been altered to varying extent under subgreenschist-facies conditions, and were replaced by Chl, Prh, Pmp, Ser and Cal. Pl-phenocrysts are idiomorphic and, if well preserved, zoning and twinning can be observed. Microprobe-analysis of the large phenocrysts revealed bytownite-composition in the cores and andesine composition at the rims. Varying Ab-contents are responsible for the oscillatory zoning of Pl. Pl is commonly replaced by fine-grained Ser and subordinate Chl and Cal. Fsp-inclusions in other large grains (e.g. Am or Grt) are Kfs. Am forms inclusion-rich, idiomorphic brown-pleochroic grains, which are sometimes intergrown with Bt. Some crystals show a color zoning, which is considered as a magmatic feature. Chemical analysis revealed ferro-tschermakitic to tschermakitic composition typical of magmatic Am. Ti-rich, randomly oriented Bt-grains show a dark to light brown pleochroism and are mostly euhedral or subhedral. Cal, Chl and opaque minerals form frequently pseudomorphs after Bt.

Up to 2.5–3 cm sized Grt-crystals are inclusion-rich (Fig. 3c). Microprobe analysis gave an average Grt composition of 60% Alm, around 15% Grs, 15% Prp, and 5% Sps. An element distribution profile (Fig. 4) shows a homogeneous element distribution (nearly constant values for Ca, Mn, Fe and Mg), which is typical for magmatic Grt together with relatively high Mn-contents. Within Grt, inclusions of Kfs (orthoclase) were observed. Ap, which has not been affected by subgreenschist-facies alteration, and Ti-rich Ilm are frequent accessory minerals.

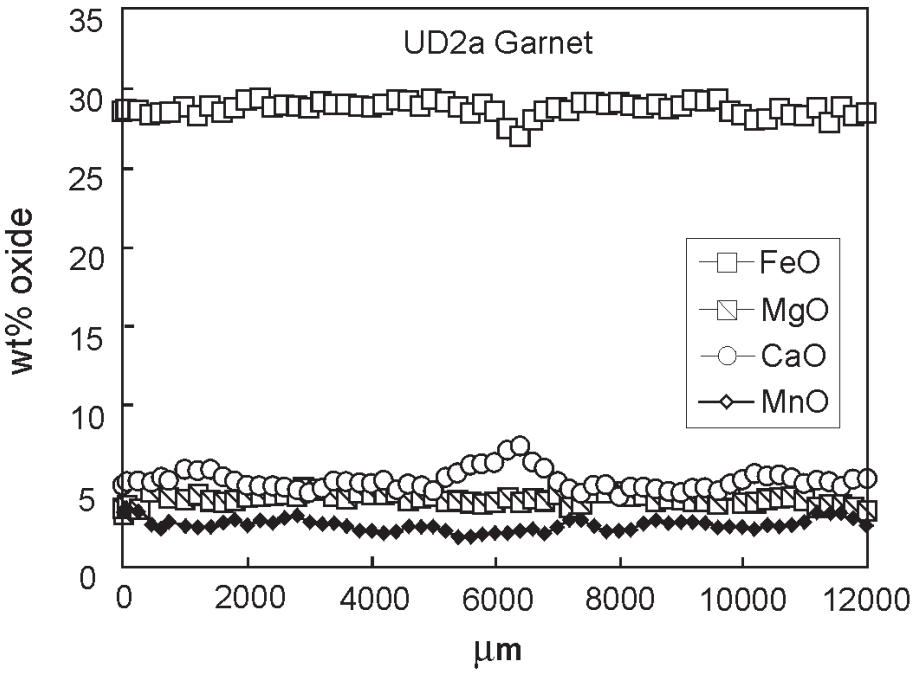


Fig. 4: Element distribution profile of Grt form andesitic dyke (sample UD2a-98).

## 3. Deformation history

The following abbreviations are used:

$D_n$ previous, currently unknown deformation event(s).
$D_{n+x}$ where x indicates the number of specific deformation phases in their relative chronological order.
$S_{n+x}$ indicates foliation planes of $D_{n+x}$
$L_{n+x}$ mineral lineation on $S_{n+x}$ planes
$F_{n+x}$ fold axis

### 3.1 Dn+1

The relatively oldest structures can be observed within cores of large Grt crystals in metapelites, i.e. Grt1: Fine-grained pigment traces the shape of euhedral Grt-grains (Fig. 3a), whereas the pigment within the matrix is recrystallised. Thus, the structures observed in Grt cores are interpreted as a pre-existing fabric overgrown by Grt during a subsequent prograde stage of metamorphism. This pre-Grt1 fabric could be either related to the early eo-Alpine subduction stage or to a pre-Alpine deformation phase. Macroscopically, no structures can be assigned to this event.

### 3.2 Dn+2

The first pervasive deformation event $D_{n+2}$ forms a compositional layering and a mylonitic foliation $S_{n+2}$ in most rock types. This foliation is characterised by the planar orientation of platy minerals, e.g. mica or platy Qtz-aggregates, but also prismatic minerals like Am and Czo in eclogite-amphibolites or large Kfs-crystals in orthogneisses. Deformation focuses in $D_{n+2}$–shear zones (parallel to $S_{n+2}$), indicating heterogeneity of this deformation phase (Fig. 3d). Macroscopically, a roughly E-W trending mineral and/or stretching lineation $L_{n+2}$ can be observed on $S_{n+2}$–surfaces. Competent layers, especially eclogite-amphibolites are boudinaged along $S_{n+2}$–surfaces perpendicular and parallel to $L_{n+2}$. Kinematic interpretation of $D_{n+2}$ is unclear because (i) most shear sense indicators have been overprinted by the subsequent, still highly ductile deformation phase $D_{n+3}$ and (ii) $D_{n+2}$–shear has been refolded parallel to $L_{n+2}$ locally inverting the shear sense. However, top to the E kinematic indicators are dominant.

Within metapelites, St and Ky grow syn- to postkinematically to $D_{n+2}$. They preserve an internal foliation, which is defined mainly by opaque minerals. This internal foliation is frequently oriented obliquely to the foliation in the matrix ($S_{n+3}$). Moreover, Pl, Grt2 and Wm also contain similar inclusion trails, indicating a roughly contemporaneous growth along with Ky and St. Grt2 crystals show curved inclusion trails of mainly Qtz and Gr indicating synkinematic growth of Grt during rotation. The orientation of the internal foliation is extremely variable in different grains, and therefore cannot be interpreted as relics of a crenulation cleavage. Bt-Am-orthogneisses (hornblende-garben schists) develop most pervasively $L_{n+2}$, formed by parallel orientation of Pl, Qtz and Bt. Am-crystals are oriented parallel to $S_{n+3}$, but not necessarily parallel to $L_{n+2}$.

### 3.3 Dn+3

During $D_{n+3}$, large-scale similar folds with subhorizontal, E-W trending fold axes develop. These S-vergent, tight to isoclinal folds are accompanied by an axial plane cleavage $S_{n+3}$, which eventually forms the prominent foliation in more incompetent lithologies (Fig. 3e). Folds of 2$^{nd}$ order are frequently developed in incompetent layers, whereas more competent, m-thick Wm-orthogneiss layers often only show 1$^{st}$ order folds and internal crenulation cleavage.

$D_{n+3}$ formed under amphibolite facies conditions, which is indicated by the recrystallisation of Pl during/post $D_{n+3}$, documented by large Pl-grains, which grow across $D_{n+3}$ microlithons. Moreover, amphibolite facies minerals like St and Ky are deformed, but not replaced by retrograde minerals during $D_{n+3}$. Some extremely Ky-rich layers show (sometimes isoclinal) folding of Ky-crystals. Bt-crystals in the immediate vicinity of the grain do not show any kinking, suggesting that T-conditions were still high enough for Bt to recrystallise, while Ky could not recover after this deformation.

### 3.4 Dn+4

This deformation event forms a crenulation cleavage with NNW-SSE trending fold axes with subvertical axial planes. $D_{n+4}$–structures develop only within mica-rich layers, where they overprint $D_{n+3}$ fold structures. Bt and Qtz recrystallise dynamically, whereas Pl develops brittle fractures. Intense growth of Chl in $D_{n+4}$ fold hinges suggests greenschist facies conditions for this event.

### 3.5 Dn+5

Numerous brittle/ductile flanking structures (Passchier 2001, Grasemann and Stüwe, 2001) overprint the $D_{n+4}$–crenulation cleavages. Within paragneisses with strong planar foliation, some flanking structures around Qtz-veins or fractures can be described as n-type flanking folds. Qtz shows dynamic recrystallisation, whereas Pl and Bt are fractured and kinked indicating T around 300°C for this deformation phase. The orientation of shear bands is not consistent over the area of investigation, but forms a conjugate, NE-SW directed extensional system (Fig. 5), which might be interpreted as a result of general shear flow with a high pure shear component.

### 3.6 Dn+6

In general, this deformation phase comprises numerous brittle faults associated with pseudotachylites and/or cohesive ultracataclasites. These brittle faults transect all pre-existing structures. Some Qtz-veins within the faulted Wm-orthogneisses still deform by dislocation glide (sample UD82–99). Qtz forms parallel, 0.05–0.5 mm thin layers or domains, which are characterised by different orientation of their c-axis. These domains are extremely consistent over the whole length of the thin section and have sharp, straight grain boundaries (Fig. 3f). The formation of this fabric presumably took place under temperatures around 300°C, where slip on Qtz-basal planes in <a>-directions is the most important mechanism (e.g. Passchier and Trouw 1996). Other Qtz-grains close to the wall rock deform by kinking and fracturing. The immediate wall rock of the Qtz-vein consists of Bt, Pl and Qtz. Sharp brittle faults transect the rock, sometimes associated with ultracataclasites/pseudotachylites demonstrating that pseudotachylites and Qtz-ultramylonites are the products of the same deformation phase. Kinematic indicators (rotated clasts, secondary cleavages and quartz textures) suggest a top to the SW sense of shear. Reverse shear bands indicate co-rotation of a co-shearing secondary fault in general shear-regime (Grasemann et al. 2003).

The unfoliated andesitic dyke is transected by numerous $D_{n+6}$ brittle faults. These are predominantly steep N-S trending normal and sinistral strike slip faults, but also subordinate low-angle, N-dipping thrusts with a top to the south sense of shear. Structural relationship suggests that the dyke intruded into a pre-existing, N-S trending brittle fault zone, which consisted at least partly of pseudotachylite-surfaces. Some pseudotachylites crosscut the cataclastic host rock, but leave the plutonic body unaffected. Nevertheless,

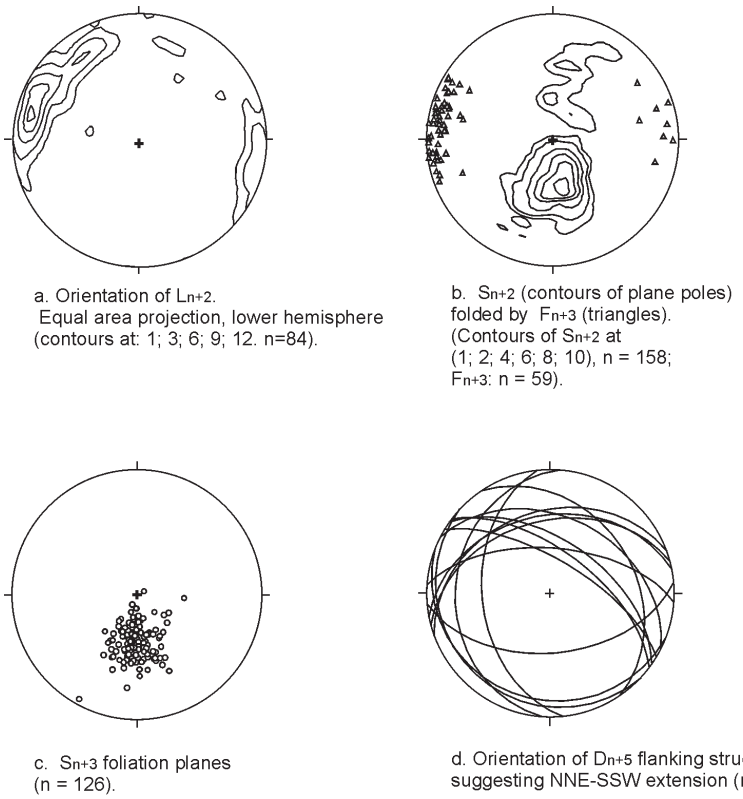

a. Orientation of $L_{n+2}$.
Equal area projection, lower hemisphere
(contours at: 1; 3; 6; 9; 12. n=84).

b. $S_{n+2}$ (contours of plane poles)
folded by $F_{n+3}$ (triangles).
(Contours of $S_{n+2}$ at
(1; 2; 4; 6; 8; 10), n = 158;
$F_{n+3}$: n = 59).

c. $S_{n+3}$ foliation planes
(n = 126).

d. Orientation of $D_{n+5}$ flanking structures,
suggesting NNE-SSW extension (n=14).

Fig. 5: Stereographic plots of structural field data.

several later faults transect the dyke, thus forming a domino-like outcrop pattern of several meters long dyke-segments. Consequently, the activity of the fault system pre- and post-dates the intrusion of the andesitic dyke.

Because of the close kinematic relationship to the sinistral strike-slip faulting of the Passeier Line the $D_{n+6}$ deformation is suggested to be related to this period of tectonic activity (compare MÜLLER et al. 2001).

## 4. Geochronological results:

All isotope analyses have been performed at the Laboratory of Geochronology of the Institute of Geology, University of Vienna. Rb and Sr isotope compositions were measured with a M30 (Micromass) single collector, whereas Sm and Nd isotopes were measured with a FINNIGAN MAT262 multicollector spectrometer. Sample digestion and element separation closely followed the procedure described by THÖNI and JAGOUTZ (1992).

### 4.1 Orthogneisses: Rb-Sr Data

Earlier authors (e.g. HOINKES 1981) considered the eo-Alpine event as being a static recrystallisation of amphibolite-facies minerals, but regarded all major deformation phases as being of pre-Alpine age. This view is in strong contradiction to field evidence and

geochronological data, since all analysed micas with eo-Alpine ages are aligned parallel to the main foliation (e.g. Spalla 1993, Sölva et al. 2001). Some high-pressure minerals show pre- to synkinematic growth, whereas other individuals of the same minerals are interkinematic, relative to $S_{n+2}$–foliation. Ongoing (re-) crystallization of Wm, Bt and Pl after $D_{n+2}$, parallel to $S_{n+3}$, is observed in all lithologies.

### 4.1.1 Wm-orthogneiss UD 49–98

Two mica-fractions and the whole rock of sample UD49–98, forming a concordant Wm-orthogneiss layer within the metasediments, were analysed. The mineral assemblage consists of Qtz, Kfs, Pl and Wm; Grt and Ap are abundant accessory minerals. Sample UD49–98 shows two different grain-sizes of Wm. Therefore two separate grain sizes have been analysed in order to detect differences in Wm age. Wm shows no significant alteration and no intergrowth with Bt. The isochron diagram (Fig. 6) shows a clearly younger age of 78.7 ±1.2 Ma for the fine-grained fraction, while the coarse Wm gives an age of 90.3 ±1.3 Ma. This data is identical with published data from the wider study area (Thöni 1999 and data referenced therein). The age of the younger, fine-grained fraction is interpreted as a product of ongoing recrystallisation of Wm below the blocking temperature, whereas the age of the coarse-grained fraction may be related to closure of the Rb-Sr isotopic system close to the metamorphic peak.

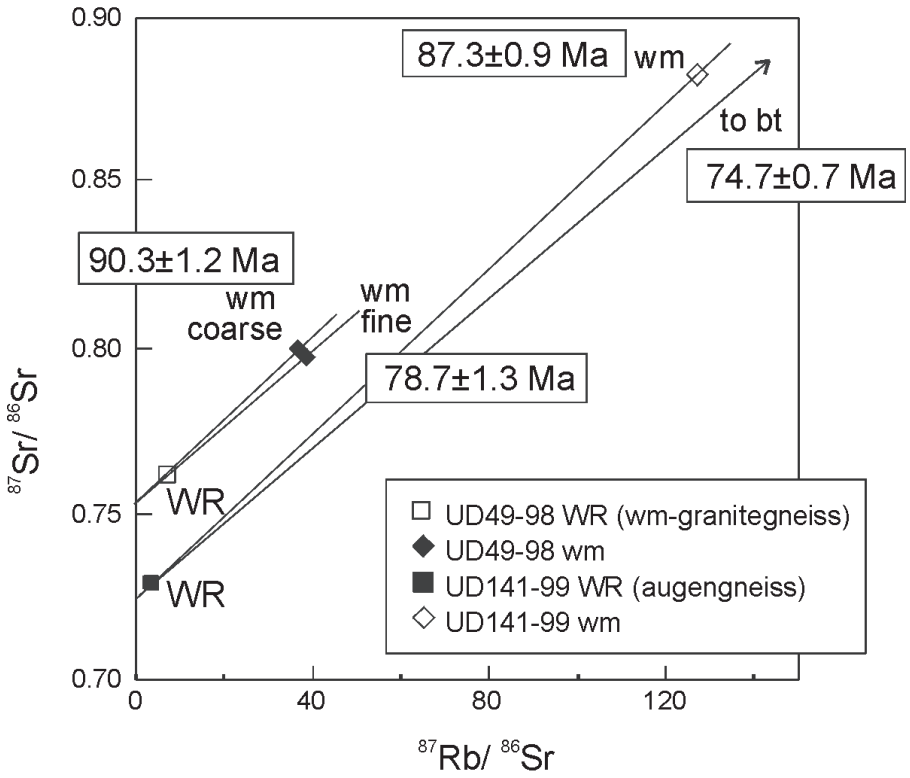


Fig. 6: Rb-Sr isochron diagram for orthogneiss samples. Only data points for Wm and WR are shown, Bt plots outside the diagram (see Tab. 2)

Tab. 2a: Rb-Sr analytical results for 2 orthogneiss samples (UD 49-98, UD 141-99) and one andesitic dyke sample (UD 71-99).

| Sample | Rb [ppm] | Sr [ppm] | 87Rb/86Sr | 87Sr/86Sr ±2s m | age |
|---|---|---|---|---|---|
| | | | | | |
| UD49-98 WR | 201.2 | 80.41 | 7.2793 | 0.762073 ±15 | |
| UD49-98 Wm (0.3-1.0) | 690.8 | 54.94 | 36.716 | 0.799852 ±15 | 90.3±1.2 |
| UD49-98 Wm (0.15-.3) | 624.0 | 46.97 | 38.779 | 0.797309 ±36 | 78.7±1.3 |
| | | | | | |
| UD141/99 WR | 162.3 | 147.6 | 3.1904 | 0.729456 ±4 | |
| UD141/99 Wm (0.2-0.4) | 497.5 | 11.53 | 127.06 | 0.883217 ±37 | 87.3±0.9 |
| UD141-99 Bt (0.2-0.4) | 793.3 | 3.620 | 680.18 | 1.448010 ±294 | 74.7±0.8 |
| | | | | | |
| UD71/99 WR | 168.1 | 243.1 | 2.0022 | 0.711798 ±5 | |
| UD71-99 Bt (>0.15) | 354.3 | 37.01 | 27.749 | 0.723688 ±21 | 32.5±0.7 |

Tab. 2b: Sm-Nd analytical results for Grt-fractions and WR from andesitic dyke sample (UD 40-98).

| | Sm [ppm] | Nd [ppm] | 147Sm/144Nd | 143Nd/144Nd±2s m | t calculated rel. to grt | $\varepsilon$ Nd, 33.3 Ma |
|---|---|---|---|---|---|---|
| | | | | | | |
| UD40-98 grt | 5.955 | 2.857 | 1.25998 | 0.512518±6 | 33.3±1.4 (3 points) | -6.8 |
| UD40-98 grt wash | 8.069 | 36.92 | 0.13211 | 0.512273±8 | 33.3±3.4 | |
| UD40-98 grt+inclusions | 4.752 | 6.852 | 0.87169 | 0.512431±8 | 34.4±4.1 | |
| UD40-98 whole rock | 4.466 | 22.79 | 0.11849 | 0.512259±3 | 34.8±1.0 | -6.52 |

### 4.1.2 Two-mica orthogneiss UD141–99

This sample was taken from a Tschigot-type orthogneiss stock E of lake Obisell. The main mineralogical components of this type of orthogneiss are Qtz, large Kfs-porphyroblasts, minor Pl and medium-grained Bt and (presumably phengite-rich) Wm. Wm from this sample yielded an WR-mineral age of 87.3 ± 0.9 Ma, which is well in line with the coarse-grained fraction of sample UD49–98 as well as several published results from the adjoining area. Bt was also analysed, and gave a significantly younger age of 74.7 ± 0.7 Ma (Fig. 6) reflecting the different blocking temperatures of the two micas for the Rb-Sr system (Armstrong et al. 1966). These data confirm the interpretation that the new ages date an evolutionary stage close to the temperature peak of eo-Alpine metamorphism. A rough estimation of a cooling rate for the temperature range of 500–300°C is possible from sample UD141–99 giving approximately 18°C/Ma. This value is in line with previous estimates of cooling rates of 10–20°C/Ma (Sölva et al. 2001).

## 4.2 Dyke: Rb-Sr and Sm-Nd Data

Geochronological investigations were also performed on an andesitic dyke, which does not show any of the deformation events preserved in the surrounding ortho- and paragneisses. Only the late brittle deformation has affected the body to some extent. Most parts of this dyke were affected by intense autohydrothermal alteration, thus Fsp and Am phenocrysts are replaced largely by Ep and Chl. However, in some places Bt and Grt have been completely preserved.

### 4.2.1 Grt from sample UD40–98

The investigated Grt forms fairly inclusion-free distinct grains up to 2.5 cm in diameter. The analyzed Grt fractions have been separated by hand-picking from a 0.15–0.3 mm sieve

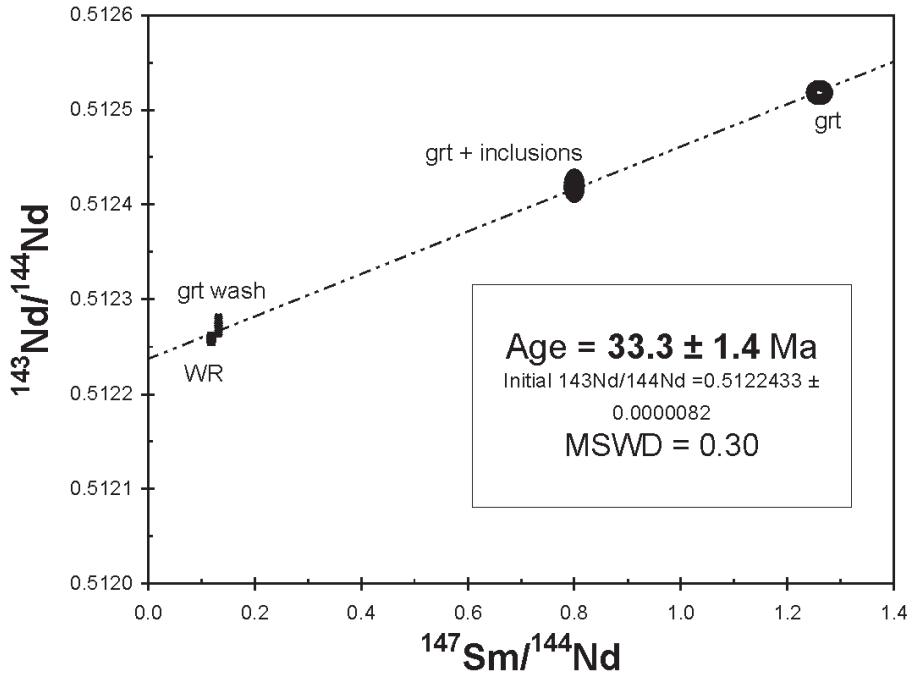


Fig. 7: Sm-Nd isochron diagram, showing different fractions of grt and the data point for the WR from dyke-sample UD40–98. Symbol size exceeds analytical errors. The data point for the WR has not been included in the age calculation (see text).

fraction. The three data points shown on Fig. 7 (i.e. clean Grt, inclusion-rich Grt and the washing solution of the clean Grt fraction) yield a best-fit isochron with an age of 33.3 ± 1.4 Ma (MSWD = 0.30). This age is interpreted as magmatic crystallization age (Fig. 7). The data point for the washing solution of the clean Grt may represent the Sm-Nd budget of both undetected microinclusions (like apatite), as well as minor intergrowths with extraneous phases. If the data point for the strongly altered WR is also included in the regression, the age result is 34.3 ± 4.2 Ma, showing considerable excess scatter, however (MSWD = 4.2, errorchron). The Depleted Mantle (DM) model age ($t_{DM}$) for the WR sample of this dyke is 1.25 Ga. The clearly negative e-Nd value of -6.5 indicates a strong crustal component in the melt, which is in line with the relatively radiogenic $^{87}Sr/^{86}Sr$ initial ratio of sample UD71–99 (Fig. 8).

### 4.2.2 Bt from dyke sample UD71–99

Bt and the whole rock from this Bt-rich sample have been analyzed with the Rb-Sr method. The Bt-WR Rb-Sr age lies at 32.5 ± 0.7 Ma (Fig. 8). The age is interpreted as giving the time of cooling below 300°C (Tc for the Rb-Sr system in biotite).

Rb-Sr and Sm-Nd ages from both dyke samples (UD 40–98 and UD71–99) overlap clearly within analytical errors, indicating that the two mineral ages may be taken as reliable values for the age of this intrusion, and further indicating rapid cooling of the magmatic body. Within errors, these results also correspond to earlier investigations of similar intrusions from the adjoining Austroalpine basement (Müller et al. 2001 and references cited therein), which further coincide with the well-known magmatic activity in Oligocene times (e.g. Dal Piaz et al. 1988).

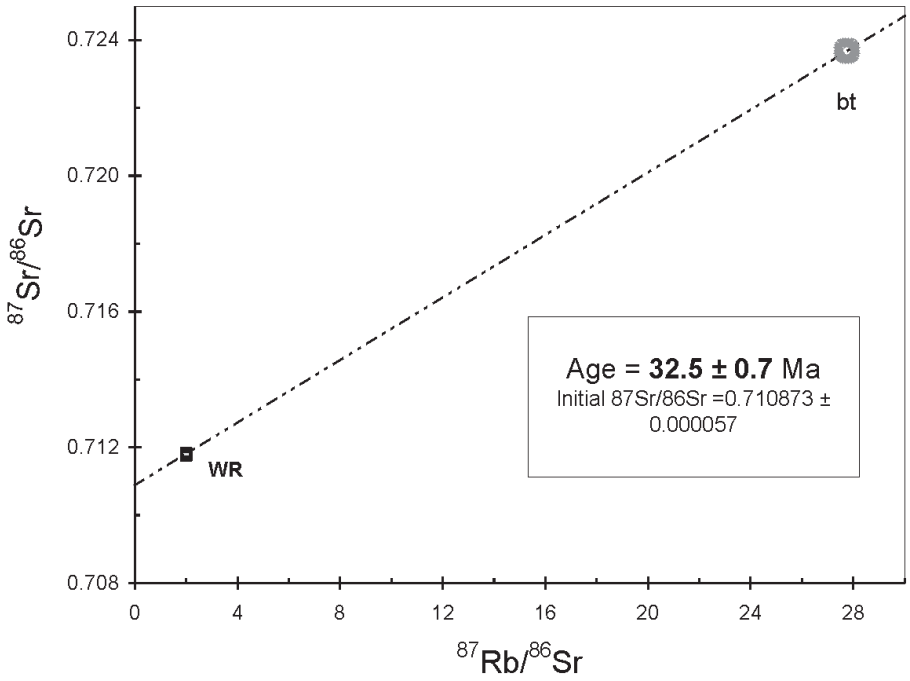


Fig. 8: Rb-Sr Bt-WR isochron plot form andesitic dyke (sample UD71–99).

## 5. Discussion

The Austroalpine unit comprises polymetamorphic basement rocks and their Mesozoic sedimentary cover sequences. Metamorphic conditions within these cover sequences mostly did not exceed lower greenschist facies conditions, whereas the basement nappes were partly subjected to amphibolite and eclogite facies conditions. Throughout the Austroalpine basement units, metabasites can be found recording eclogite facies metamorphic conditions. It is a crucial question, which orogenic cycle produced the predominant mineral assemblages and structures within the metagabbros and -basalts and their acidic host rocks.

Previous studies in the SE part of the ÖC suggested an eo-Alpine eclogite facies metamorphism (e.g. Hoinkes et al. 1991). Structural investigations (Spalla 1990, 1993, Sölva et al. 2001) showed that not only the formation of (eclogite- and) amphibolite facies mineral assemblages, but also most of the structures at all scales should be attributed to the Cretaceous HP-event and subsequent exhumation. This observation is in contrast to previous studies performed in the S and SW ÖC by van Gool et al. (1987), who assigned the major structures, especially the "Schlingen" of the Schneeberg Complex (SC), km-scale folds with subvertical fold axes, to the Variscan metamorphic cycle. Nevertheless, recent geochronological and petrological studies on the large- and small-scale structures in the NE part of the SC confirmed the exclusively eo-Alpine P-dominated metamorphism of this unit (Habler et al. 2000).

In contrast to the monometamorphic SC, the rocks in the area of investigation are part of the polymetamorphic ÖC and, accordingly, some authors have differentiated pre-Alpine mineral generations (Hoinkes 1981, Spalla 1993). In the study area, $D_{n+1}$–

structures inside large Grt-crystals preserve an older fabric, which might be interpreted as relicts of either a pre-Alpine deformation or, alternatively, of an early stage of Alpine subduction.

The first penetrative deformation event in the rocks of the Saltaus and Fals valleys ($D_{n+2}$) forms a mylonitic foliation with an E-W trending mineral lineation. Rb-Sr dating of Wm from mylonitic orthogneisses, which show dynamic recrystallisation during this deformation, gave ages around 90 Ma. The present contribution adds new data to a series of Rb-Sr ages obtained by the analysis of coarse-grained Wm mainly from orthogneisses and some metabasites (Satir 1975, Hoinkes et al. 1991) from the southeastern ÖC, which range between 83 and 110 Ma (Thöni, 1999 and data referenced therein). The recystallisation of Wm parallel to a mylonitic foliation ($S_{n+2}$) and lineation ($L_{n+2}$) was induced by $D_{n+2}$ general shear deformation. This event is interpreted as the most effective phase for the exhumation of the HP-metabasites and their acidic host rocks.

It is generally accepted that eclogite facies rocks are formed in subduction zones, usually derived from segments of former oceanic crust. However, collision of continental plates may also lead to subduction of continental lithosphere. The latter geodynamic setting is probably valid for the occurrences of eclogites in the SE ÖC. In contrast to oceanic crust, subducted continental rocks are generally not recycled into the upper mantle, and will be exhumed, driven by buoyancy forces, after reaching a critical depth of 100–160 km (Wheeler 1991, Platt 1993, Chemenda et al. 1995). The buoyancy forces are thought to cease when the crustal rocks reach the lower boundary of the lithospheric crust of the upper plate. An effective mechanism for the exhumation of the eo-Alpine HP-rocks in the Saltaus valley and other occurrences might be the extrusion of a crustal wedge, as proposed for the Himalayas (Hodges et al. 1993, Grujic et al. 1996, Grasemann et al. 1999) and other orogens, including the Alps (Chemenda et al. 1995). Such a crustal wedge is bordered by a thrust fault at the base and a normal fault at the top, which converge at depth into a common detachment. This geometry admits contemporaneous activity of both normal and thrust faults in an overall transpressional regime. In the present geometry, the existence of an exhuming wedge is not easy to envisage in the SE ÖC. The rocks exposed in the SC and the SE ÖC generally show a mylonitic fabric, which was formed under eclogite and/or P-dominated amphibolite facies general shear conditions (Spalla 1993, Sölva et al. 2001). To the N of the SC, the influence of Alpine ductile deformation decreases rapidly. Moreover, N-dipping mylonitic foliations of the SC are overlain by the northern ÖC. Based on these observations, the SC is tentatively interpreted as the normal fault bordering the top of the postulated exhuming wedge.

## 6. Conclusions

In the ÖC north of Meran six deformation events with different kinematics and metamorphic conditions have been distinguished: $D_{n+1}$ structures are observed in cores of large Grt-porphyroblasts, where an older microfabric outlined by fine-grained inclusions is preserved. This fabric may be related either to an early stage of Alpine subduction, or to pre-Alpine metamorphism. The subsequent phases are interpreted as being eo-Alpine in age, based on geochronological data and relative age relationships. $D_{n+2}$ is the first penetrative deformation event related to the exhumation of the eclogitic bodies and dominated by non-coaxial flow. Dating of white mica and biotite, which are aligned parallel to these structures in orthogneisses, gave an eo-Alpine age for this event. $D_{n+3}$ deformed the pre-existing structures by large-scale S-vergent folds with a N dipping axial plane cleavage and subhorizontal E-W trending fold axes und amphibolite facies conditions.

Post-dating the three deformation events associated with the emplacement of the HP rocks, three additional deformation phases document the transition to brittle/ductile

regimes. During $D_{n+4}$, a NNW-SSE trending crenulation cleavage develops in mica-rich layers. This is probably related to regional transpression during a late stage of exhumation. $D_{n+5}$–structures are interpreted as flanking structures, formed during a phase of regional NE-SW directed extension with a high pure shear component. $D_{n+6}$–brittle faulting is related to Tertiary movements along the Passeier and Jaufen Line, documented by N-S trending faults, which are often associated with pseudotachylites and ultracataclasites, but also with low-T quartz-ultramylonites. This deformation is accompanied by the intrusion of an andesitic dyke. Bt and Grt from this magmaitc body have been dated by Rb-Sr and Sm-Nd methods, respectively. Mineral ages around 33 Ma are well in line with data for the Periadriatic magmatism along the Alpine chain.

## Acknowledgements

Monika Jelenc performed the Rb-Sr analytical work. The authors would like to thank Gerlinde Habler, Helmuth Sölva, Rasmus Thiede, Florian Fusseis and Manfred Linner for informative discussions in the course of this study. The work has been supported by the Austrian Science Fund FWF (P-13227–GEO and P-15668–GEO) and the ETH-project 0–20998–02. We gratefully acknowledge the helpful and rapid review by Richard Spiess.

## References

Armstrong R. L., Jäger E., Eberhardt P. 1966: A comparison of K-Ar and Rb-Sr ages on Alpine biotites. – Earth and Planetary Science Letters, 1, 13–19.

Chemenda A. I., Mattauer M., Malavieille J., Bokun, A. N. 1995: A mechanism for syn-collisional deep rock exhumation and associated normal faulting: results from physical modelling. – Earth and Planetary Science Letters, 132, 225–232.

Dal Piaz G. V., Del Moro, A., Martin, S., Venturelli, G. 1988: – Post-collisional Magmatism in the Ortler-Cevedale Massif (Northern Italy). Jb. Geol. B.-A. 131, 533–551.

Froitzheim N., Conti P., van Daalen M. 1997: Late Cretaceous, synorogenic, low-angle normal faulting along the Schlinig fault (Switzerland, Italy, Austria) and its significance for the tectonics of the Eastern Alps. – Tectonophysics, 280, 267–293.

Grasemann B., Fritz H., Vannay J.-C. 1999: Quantitative kinematic flow analysis from the Main Central Thrust Zone (NW-Himalaya India): implications for a decelerating strain path and the extrusion of orogenic wedges. – Journal of Structural Geology 21(7), 837–853.

Grasemann B., Stüwe K. 2001: The development of flanking folds during simple shear and their use as kinematic indicators. – Journal of Structural Geology 23(4), 715–724.

Grasemann B., Stüwe K., Vannay J.-C. 2003: Sense and non-sense of shear in shear band and flanking fold structures. – Journal of Structural Geology 25(1), 19–34.

Grujic D., Casey M., Davidson C., Hollister L. S., Kündig R., Pavlis T., Schmid S. 1996: Ductile extrusion of the Higher Himalayan Crystalline in Bhutan: evidence from the quartz microfabrics. – Tectonophysics 260, 21–43.

Habler G., Linner M., Thiede R., Thöni, M. 2000: Eo-Alpine Metamorphism in the Upper Austroalpine Schneeberg Complex (Eastern Alps, Italy / Austria): Constraints on the P-T-t-D Evolution during Decompression. – Terra nostra 2000(5), 23.

Helbig P., Schmidt K. 1978: Zur Tektonik und Petrogenese am W-Ende des Schneeberger Zuges (Ostalpen). – Jahrbuch der Geologischen Bundesanstalt 121/2, 177–217.

Hodges K. V., Burchfiel B. C., Royden L. H., Chen Z., Liu Y. 1993: The metamorphic signature of contemporaneous extension and shortening in the central Himalayan orogen: data from Nyalam transect, southern Tibet. – Journal of Metamorphic Geology 11, 721–737.

Hoinkes G. 1981: Mineralreaktionen und Metamorphosebedingungen in Metapeliten des westlichen Schneebergerzuges und des angrenzenden Altkristallins (Ötztaler Alpen). – Tschermaks Mineralogische und Petrographische Mitteilungen 28, 31–54.

Hoinkes G., Kostner A., Thöni M. 1991: Petrologic Constraints for Eoalpine Eclogite Facies Metamorphism in the Austroalpine Ötztal Basement. – Mineralogy and Petrology 43, 237–254.

Hoinkes G., Thöni, M. 1987: New findings of eclogites within the eoalpine amphibolite grade area of the Ötztal basement. – Terra cognita 7, 96.

Hollister L. S., Crawford M. L. 1986: Melt-enhanced deformation: A major tectonic process. – Geology 14, 558–561.
Kretz R. 1983: Symbols for rock-forming minerals. – American Mineralogist 68, 277–279.
Miller C., Schuster R., Klötzli U., Frank W., Purtscheller F. 1999: Post-collisional potassic and ultrapotassic magmatism in SW Tibet: geochemical and Sr-Nd-Pb-O isotopic constraints for mantle source characteristics and petrogenesis. – Journal of Petrology, 40, 1399–1424.
Müller W., Prosser G., Mancktelow N. S., Villa I. M., Kelley S. P., Viola, G., Oberli, F. 2001: Geochronological constraints on the evolution of the Periadriatic Fault System (Alps). – International Journal of Earth Sciences 90(3), 623–653.
Passchier C. W. 2001: Flanking structures. – Journal of Structural Geology 23, 951–962.
Passchier C. W., Trouw, R.A.J. 1996: Microtectonics. – Spriger-Verlag.
Platt J. P. 1993: Exhumation of high-pressure rocks: a review of concepts and processes. – Terra Nova 5, 119–133.
Purtscheller F., Haas R., Hoinkes G., Mogessie, A., Tessardi, R., Veltman, C. 1987: Eoalpine metamorphism in the crystalline basement. – In: Geodynamics of the Eastern Alps (edited by Flügel, H. W., Faupl, P.). Deuticke, Wien, 185–170.
Rosenberg C., Berger, A., Schmid, S. M. 1995: Observations from the floor of a granitoid pluton: a constraint on the driving force of final emplacement. – Geology 23, 443–446.
Satir M. 1975: Die Entwicklungsgeschichte der westlichen hohen Tauern und der südlichen Ötztal-Masse auf Grund radiometrischer Altersbestimmungen. – Mem. Inst. Geol. Min. Univ. Padova 30, 1–84.
Schmid S. M., Haas, R., 1989: Transition from near-surface thrusting to intrabasement decollement, Schlining thrust, Eastern Alps. – Tectonics, 8, 697–718.
Sölva H., Thöni M., Grasemann, B., Linner, M. 2001: Emplacement of eo-Alpine high-pressure rocks in the Austroalpine Ötztal complex (Texel group, Italy/Austria). – Geodinamica Acta 14, 345–360.
Spalla M. I. 1990: Polyphased deformation during uplifting of metamorphic rocks: the example of the deformational history of the Texel Gruppe (Central-Western Austroalpine Domain of the Italian Eastern Alps). – Mem. Soc. Geol. It. 45, 125–134.
Spalla M. I. 1993: Microstructural control on the P-T path construction in metapelites from the Austroalpine crust (Texel Gruppe, Eastern Alps). – Schweiz. Mineral. Petrogr. Mitt. 73, 259–275.
Spiess R. 1995: The Passeier-Jaufen Line: a tectonic boundary between Variscan and eo-Alpine Meran-Mauls basement. – Schweiz. Mineral. Petrogr. Mitt. 75, 413–425.
Steenken, A., Siegesmund, S., Heinrichs, T. 2000: The emplacement of the Rieserferner Pluton (Eastern Alps, Tyrol): constraints from field observations, magnetic fabrics and microstructures. – Journal of Structural Geology 22, 1855–1873.
Thöni M. 1981: Degree and evolution of the Alpine metamorphism in the Austroalpine Unit W of the Hohe Tauern in the light of K/Ar and Rb/Sr age determination. – Jahrbuch der Geologischen Bundesanstalt 124(1), 111–174.
Thöni, M. 1999: A review of geochronological data from the Eastern Alps. – Schweiz. Mineral. Petrogr. Mitt. 79, 209–230.
Thöni M., Jagoutz, E. 1992: Some new aspects of dating eclogites in orogenic belts: Sm-Nd, Rb-Sr and Pb-Pb isotopic results form the Austroalpine Saualpe and Koralpe type-locality (Carinthia/Styria, SE Austria). – Geochim. Cosmochimica Acta 56, 347–368.
Van Gool, J. A. M., Kemme, M. M. J., Schreurs, G. M. M. F. 1987: Structural investigations along an E-W cross-section in the southern Ötztal Alps. – In: Geodynamics of the eastern Alps (edited by Flügel, H. W., Faupl, P.), 190–199.
Von Blanckenburg F., Hagami H., Deutsch, A., Oberli, F., Meier, M., Wiedenbeck, M., Barth, S., Fischer, H. 1998: The origin of Alpine plutons along the Periadriatic Lineament. – Schweiz. Mineral. Petrogr. Mitt. 78, 55–66.
Wheeler J. 1991: Structural evolution of a subducted continental sliver: the northern Dora Maira massif, Italian Alps. – Journal of the Geological Society London 148, 1101–1113.